

High-Resolution Peak Demand Estimation Using Generalized Additive Models and Deep Neural Networks

Jonathan Berrisch^a, Michał Narajewski^a, Florian Ziel^a

^aUniversity of Duisburg-Essen, Germany

Abstract

This paper covers predicting high-resolution electricity peak demand features given lower-resolution data. This is a relevant setup as it answers whether limited higher-resolution monitoring helps to estimate future high-resolution peak loads when the high-resolution data is no longer available. That question is particularly interesting for network operators considering replacing high-resolution monitoring predictive models due to economic considerations. We propose models to predict half-hourly minima and maxima of high-resolution (every minute) electricity load data while model inputs are of a lower resolution (30 minutes). We combine predictions of generalized additive models (GAM) and deep artificial neural networks (DNN), which are popular in load forecasting. We extensively analyze the prediction models, including the input parameters' importance, focusing on load, weather, and seasonal effects. The proposed method won a data competition organized by Western Power Distribution, a British distribution network operator. In addition, we provide a rigorous evaluation study that goes beyond the competition frame to analyze the models' robustness. The results show that the proposed methods are superior to the competition benchmark concerning the out-of-sample root mean squared error (RMSE). This holds regarding the competition month and the supplementary evaluation study, which covers an additional eleven months. Overall, our proposed model combination reduces the out-of-sample RMSE by 57.4% compared to the benchmark.

Keywords: Electricity Peak Load, Generalized Additive Models, Artificial Neural Networks, Prediction, Combination, Weather Effects, Seasonality

JEL: Q41, C53

1. Introduction

The decentralization of the energy system renders accurate electricity demand forecasts more critical than ever. Spikes in demand can produce strain on the networks. These issues will likely increase due to the increased use of lower-carbon technologies such as heat pumps and electric vehicles. Monitoring is expensive in the long term since it requires initial investments and sustained maintenance. Network operators are, therefore, particularly interested in peak-demand estimates.

This paper presents a winning method for high-resolution peak-demand prediction using generalized additive models (GAM) and deep neural networks (DNN). We developed this method for solving a data competition organized by Western Power Distribution (WPD), a British network operator responsible for the Midlands, South West, and Wales. The goal was to predict high-resolution minimum and maximum peak load using only low-resolution data and weather information. This is a relevant setup as it answers whether limited higher-resolution monitoring helps to estimate future high-resolution peak loads when the high-resolution data is no longer available. This is particularly interesting for network operators since consistent high-resolution monitoring is very costly [1, 2]. Therefore, replacing high-resolution monitoring with data science methods is an economically attractive scenario. If the results for a particular substation generalize to other substations, only low-resolution data would be necessary to obtain high-resolution features.

Peak load estimates are relevant at various scales. While Nationwide forecasts are essential for climate change issues and resource planning [3, 4], network operators are usually more interested in regional peak load predictions, which are also the topic of this paper. Another relevant topic for network operators is peak load shaving [5, 6]. The latter deals with flattening the load curve. While this topic is also highly relevant for network operators, it is less related to the topic of this paper. In the following paragraphs, we provide an overview of research on peak load estimation.

There are various papers dealing with peak load prediction at different scales, e.g, forecasting short-term load of individual households [7, 8], office buildings [9], low-voltage feeders [10], cities [11], and nations [4]. The results indicate that weather data like temperature, humidity, wind speeds, and air-pressure help explain peak loads [12, 13, 14, 15]. The influence of windspeed on electricity loads is discussed in detail in [16]. [17] deals with the selection of suitable weather stations. In contrast, [10], who supplemented their model with deterministic factors like the day of the week, found little to no evidence for an impact of the temperature on electricity load.

The applied techniques for peak load forecasting are diverse. They include models like time-varying autoregressive (ARTV) [18], recurrent and convolutional neural networks (RNN, CNN) [14], long-short term memory (LSTM) networks [15], gradient boosting [19], and multistep approaches [20, 21, 22]. The techniques proposed in this paper have also been applied to load forecasting. GAMs are widely used in global [23] and local [24, 25] short-term electricity load forecasting, and in forecasting high-resolution demand smart-meter data [26]. The literature on artificial intelligence

models based on neural networks in electricity load forecasting is much broader. A wide range of artificial neural networks, including multilayer perceptron networks (MLP), CNNs, and RNNs, are used in peak load [27, 28] and load [29, 30, 31, 32, 33, 34, 35, 36] forecasting.

Summarizing the research contribution of this manuscript, we

- i) propose a winning method for predicting high-resolution power load with low-resolution data.
- ii) analyze the descriptive data characteristics of relevant input data (esp. load and weather inputs) in detail for suitable usage for predictive analytics.
- iii) design machine learning models, GAMs and DNNs, which combined yield the best performance among competitors.
- iv) provide a rigorous predicting study that ensures the robustness of the method.
- v) study and interpret the explanatory power of relevant inputs and discuss hyperparameter tuning results.

The remainder of this paper is structured as follows. Section 2 introduces the data and provides an extensive descriptive data analysis. Section 3 describes the models that we developed. The models' performance is measured using an evaluation study. Section 4 contains the study design as well as the results. Section 5 concludes.

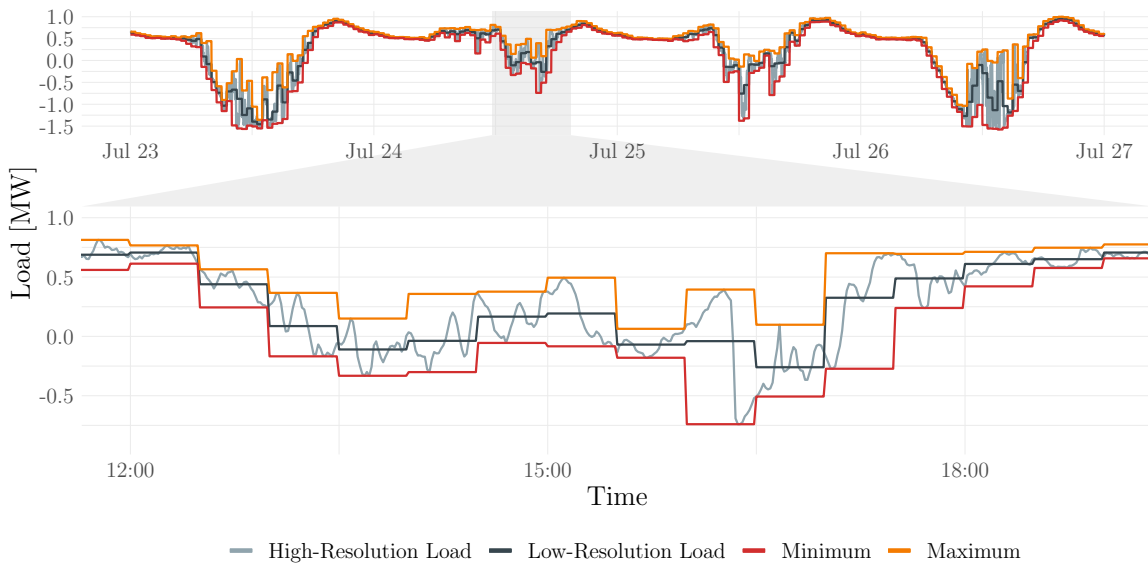


Figure 1: Illustration of the high-resolution peak load estimation task for four days in July 2021. The half-hourly minima and maxima (red, orange) of the high-resolution 1-minute load data (grey) have to be predicted using the low-resolution half-hourly load values (black).

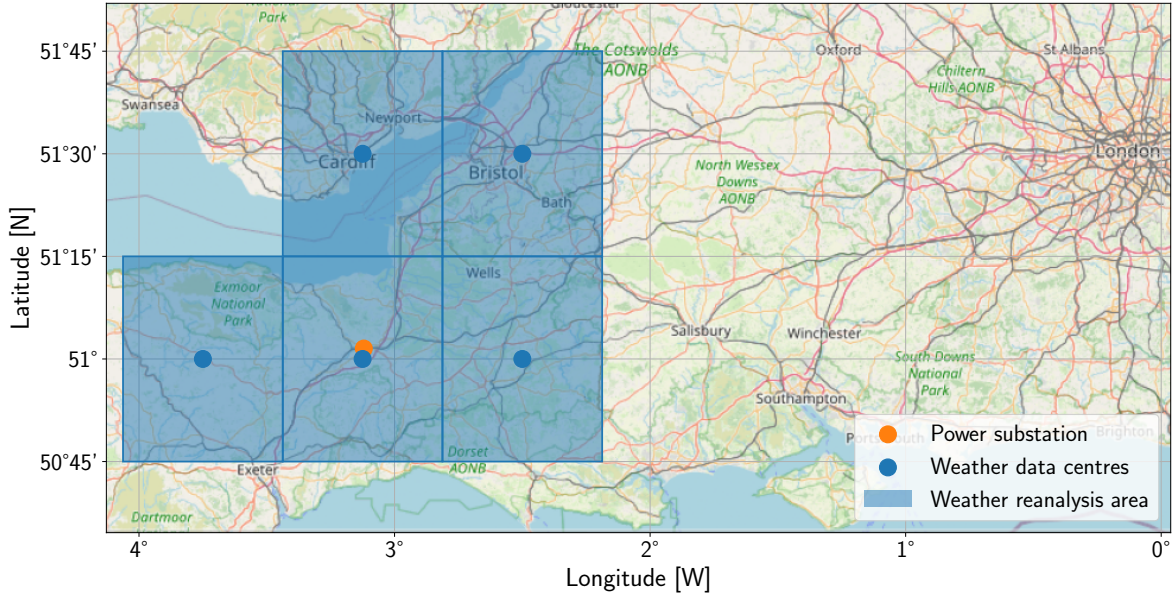


Figure 2: Location of the considered power substation and weather reanalysis data in the south-west of England. The map was generated using OpenStreetMap.

2. Setting, Data & Exploratory Analysis

We consider a data set of the high-resolution peak load estimation challenge ranging from November 2019 to September 2021, covering almost two years of data. The data was provided by WPD¹. Next to the mentioned load data that is also illustrated in Fig. 1, weather data was given to improve predictions. This is MERRA-2 weather reanalysis data from five areas close to the substation, as shown in Fig. 2. This weather data includes temperature (temp), solar irradiance (solar), north-south wind (windN), east-west wind (windE), pressure (press), and specific humidity (humid). We utilize the six weather inputs by averaging across the five areas.

Given the data mentioned above, the competition participants were requested to predict the minimum and maximum load values every half-hour of September 2021. However, to illustrate the robustness of the methodology used in the competition, we utilize a rolling window study with 12 test months from October 2020 to September 2021. Furthermore, the competition winner was determined by evaluating a specific skill with respect to the squared error. Thus, we are required to provide predictions of the expected value of the minimum and maximum load in each half-hour to optimize the skill score [37]. Further details on the evaluation are described in Section 4.3.

Let L_t be the half-hourly load, corresponding to the black line in Fig. 1. Further, let L_t^{\min} and L_t^{\max} be the minimum and maximum load values of the high-frequency data, which are our prediction targets. As L_t is known and it holds $L_t^{\min} < L_t < L_t^{\max}$

¹The data can be retrieved from [WPD Datasets](#)

it makes sense to model $\Delta_t^{\min} = L_t^{\min} - L_t$ and $\Delta_t^{\max} = L_t^{\max} - L_t$ directly. Fig. 3 illustrates the minimum and maximum load difference Δ_t^{\min} and Δ_t^{\max} for two selected time regions. Here, we added the discrete second order central difference (DSOCD) additionally

$$L_t'' = L_{t-1} - 2L_t + L_{t+1} \quad (1)$$

of the load L_t , as well as its negative version $-L_t''$. We observe that Δ_t^{\min} and Δ_t^{\max} tends to be larger in absolute terms if L_t'' (or a neighbouring value like L_{t-1}'' or L_{t+1}'') is large in absolute terms. Thus, it makes sense to regard L_t'' as an important feature in model engineering.

A closer look at the bottom graph in Fig. 3 shows relatively large absolute values for L_t'' in winter at the very end and beginning of a day (at 23:30 and 0:00). It concerns a limited period in the winter months exclusively. However, we can not explain those values. In contrast to other large values, those do not translate into large absolute Δ_t^{\min} and Δ_t^{\max} values. Therefore, we decided to replace these values to prevent any influence of these spurious observations on our prediction. To adjust for these phenomena, we introduce an adjusted discrete second-order central difference \tilde{L}_t'' where the corresponding linear interpolation replaces the two values. The latter is formally defined as:

$$\tilde{L}_t'' = \begin{cases} L_t'' & \text{if } t \bmod 48 = 1, \dots, 46 \\ \frac{1}{3}L_{t-2}'' + \frac{2}{3}L_{t+1}'' & \text{if } t \bmod 48 = 0 \\ \frac{2}{3}L_{t-2}'' + \frac{1}{3}L_{t+1}'' & \text{if } t \bmod 48 = 47 \end{cases}. \quad (2)$$

We define three deterministic components for further preliminary data analysis to capture potential seasonal characteristics in the data. Those are daily, weekly and annual inputs, which we refer to by D_t , W_t , and A_t . D_t and W_t count the number of hours in a day or week starting Monday. Similarly, A_t counts the number of hours in a meteorological year with 365.24 days starting at 0:00 on 1st January 2020.

Fig. 4 shows a correlation matrix of relevant data discussed above. These are load-related time series Δ_t^{\min} , Δ_t^{\max} , L_t , \tilde{L}_t'' , L_t'' , the six weather time series, and the daily, weekly and annual seasonal inputs D_t , W_t , and A_t . We illustrate Pearson's correlation coefficients on the lower triangle and the distance correlation on the upper triangle. The former is a standard linear dependency measure that takes values in $[-1, 1]$. The latter is a non-linear dependency measure that takes values in $[0, 1]$ and characterizes stochastic independence [38].

We observe that likely L_t and \tilde{L}_t'' will be important to explain Δ_t^{\min} and Δ_t^{\max} . We also see that \tilde{L}_t'' seems to be slightly preferable to L_t'' for modeling purposes. In terms of correlation, solar irradiance explains best Δ_t^{\min} and Δ_t^{\max} among all meteorological inputs, which is plausible due to the expected high impact from photovoltaic to the load. However, the overall contribution of the weather data remains unclear, especially as weather data is highly correlated with deterministic seasonal variables. Among the seasonal inputs, we observe close-to-zero correlation values between -0.04 and 0.05 . This means that there is merely and linear dependency between Δ_t^{\min} and Δ_t^{\max} and the seasonal inputs. However, we observe elevated distance correlations for the daily



Figure 3: Illustration of minimum and maximum load differences $\Delta_t^{\min} = L_t^{\min} - L_t$ and $\Delta_t^{\max} = L_t^{\max} - L_t$ with positive and negative discrete second order central difference (DSOCD) L_t'' of the load L_t for four days in summer (23-26 July 2020, top) and winter (5-8 December 2020, bottom).

and annual inputs. Since strong linear relations are already ruled out due to the close-to-zero Pearson's correlation, we can deduce that the relation between daily and annual inputs and Δ_t^{\min} and Δ_t^{\max} is non-linear.

3. Models

To preserve comparability, we design the GAM and DNN models using the same input matrix \mathbb{X} . \mathbb{X} contains $N = 21$ columns that are listed in Tab. 1. Note again that the challenge did not ask for forecasts (of the future) but for precise predictions. Therefore, in contrast to a classical forecasting problem, it is allowed to use positively lagged inputs to deduce the high-frequency peak load behavior. Therefore, we include positive lags of the load and DSOCD load.²

²However, at the end of the data set, we have to omit positively lagged components to predict the last observations of September 2021.

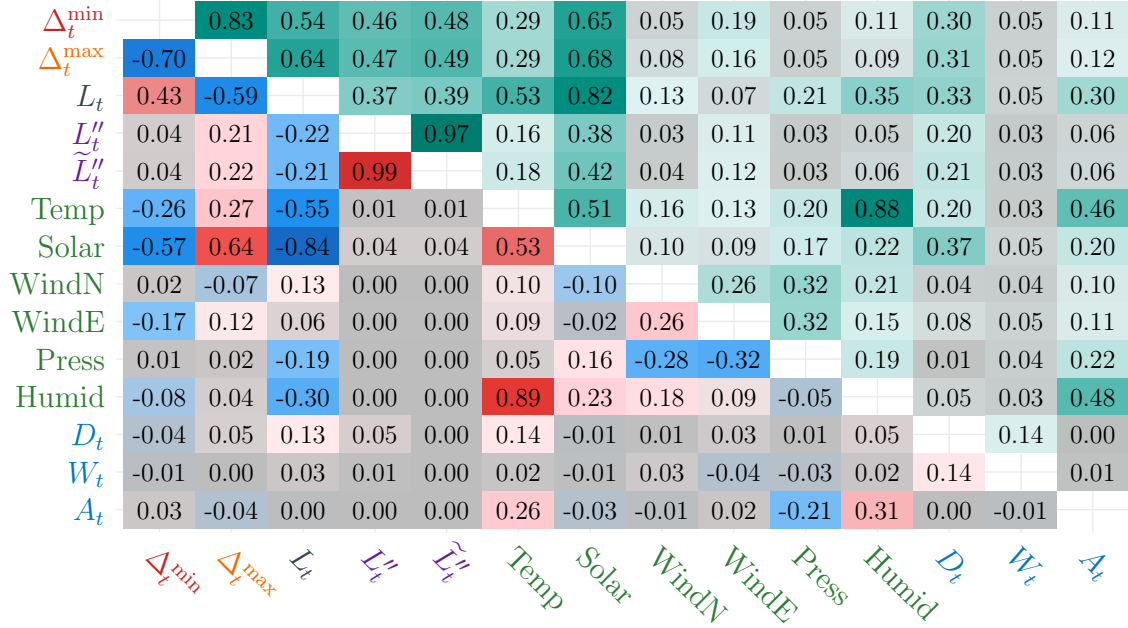


Figure 4: Correlation plot with Pearson's correlation on the lower triangle and distance correlation on the upper triangle.

Variable type	Included feature	Number
Lagged load	L_{t-1}, L_t, L_{t+1}	3
Lagged DSOCD load	$\tilde{L}_{t-4}'', \dots, \tilde{L}_{t+4}''$	9
Weather inputs	Temp, Solar, WindN, WindE, Press, Humid	6
Seasonal inputs	D_t, W_t, A_t	3

Table 1: Table of all 3+9+6+3=21 inputs.

3.1. GAM models

A generalized additive model (GAM) is a model with M additive model components. For our objectives Δ_t^{\min} and Δ_t^{\max} this is in general

$$\Delta_t^m = \sum_{i=1}^M f_i(X_{t,1}, \dots, X_{t,N}) + \varepsilon_t \quad (3)$$

where $m \in \{\min, \max\}$. The additive terms f_i may represent arbitrary model components. Traditionally, linear terms and smoothing spline components are used for f_i . However, complex building blocks like gradient boosting machines or (deep) neural networks are also used in recent years, [39, 40].

In this application, we reduce the complexity of the considered GAM model (3) by restricting the model to linear terms and 2-way interactions. Thus, we do not allow for 3-way or higher interactions between the inputs. Additionally, we use GAMs in the traditional framework using splines, more precisely cubic B-splines. The GAM model with all 2-way interactions is defined by

$$\Delta_t^m = \sum_{i=1}^N b_{k_0}(X_{t,i}) + \sum_{i=1}^N \sum_{j=1, j>i}^N b_{k_1, k_2}(X_{t,i}, X_{t,j}) + \varepsilon_t \quad (4)$$

where b_{k_0} and b_{k_1, k_2} denote univariate and bivariate splines with k_0 , and (k_1, k_2) knots. For the latter, we consider tensor interaction splines that only model joint interaction effects. In addition, we choose $k_0 = 27$ and $k_1 = k_2 = 9$. Thus, linear terms are specified by 27 parameters and bivariate terms by 81 parameters.

The model is estimated using `bam` function of the R package `mgcv` [41] which allows efficient estimation for large data sets. Here, the input data can be discretized first to reduce the computational effort in the fast restricted maximum likelihood (fREML) computation. The fREML estimation is performed with respect to the Gaussian distribution with fixed variance, which corresponds to minimizing least squares. The parameter estimation is performed so that the Bayesian information criterion (BIC) is minimized, utilizing the effective degrees of freedom of the smoothing spline components. For more details on computational and theoretical issues on spline-based GAM models see [41].

In addition to (4), we introduce a reduced GAM model (**GAM.red**) that includes only selected 2-way interactions. We consider here only interactions that involve the crucial load input L_t , the second derivative \tilde{L}_t'' and the daily seasonal term Solar_t . Thus, the reduced GAM model is

$$\begin{aligned} \Delta_t^m = & \sum_{i=1}^N b_{k_0}(X_{t,i}) + \sum_{i=2}^N b_{k_1, k_2}(L_t, X_{t,i}) \\ & + \sum_{i=3}^N b_{k_1, k_2}(\tilde{L}_t'', X_{t,i}) + \sum_{i=4}^N b_{k_1, k_2}(\text{Solar}_t, X_{t,i}) + \varepsilon_t \end{aligned} \quad (5)$$

with the same $k_0 = 27$ and $k_1 = k_2 = 9$. Note that for notation convenience in (5) we assume that in column 1 to 3 in \mathbb{X} are L_t , \tilde{L}_t'' and Solar_t . The computational cost for parameter estimation of the **GAM.red** is substantially lower than in (4). Using our eight-core machine, it relieves from about 3 hours to 2 minutes for the entire training and prediction of a minimum or maximum peak model. We also considered the main GAM models **GAM.full** and **GAM.red** with absolute wind speed³ instead of north-south and east-west components. However, the results differed only marginally (less than 0.05% in RMSE). We, therefore, decided to use the original wind components and omit to report the results for brevity⁴. The highly nonlinear structure of DNNs allows them to consider these nonlinear transformations themselves. We, therefore, decided to consider the original wind components only.

We consider the simple GAM model **GAM.simple** to illustrate the relevance and the non-linear impact of the mentioned three inputs L_t , \tilde{L}_t'' and Solar_t beyond the descriptive data analysis:

$$\Delta_t^m = b_{k_0}(L_t) + b_{k_0}(\tilde{L}_t'') + b_{k_0}(\text{Solar}_t) + \varepsilon_t \quad (6)$$

with $k_0 = 27$. The BIC-based fit of model (6) illustrated in Fig 5. We observe that especially the load L_t and the second derivative \tilde{L}_t'' have clearly non-linear relationships. The spline fit of \tilde{L}_t'' close to 0 looks approximately like an absolute value which corresponds to the effect that was already visible in Fig 3.

Finally, we also consider the GAM model (4) without any weather inputs to evaluate the impact of the weather inputs. We refer to that model as **GAM.noWeather**.

3.2. Deep neural network model

The deep neural network (DNN) model uses the MLP structure as shown in Fig. 6. Formally, for $i \in \{1, \dots, I\}$ we define it by

$$\mathbf{H}_{t,i} = a_i(\mathbf{H}_{t,i-1}\mathbf{W}_i + \mathbf{b}_i) \quad (7)$$

where $\mathbf{H}_{t,i}$ is the output matrix of i th hidden layer, and \mathbf{W}_i , \mathbf{b}_i , and a_i are the weights, bias and activation function of the i th hidden layer, respectively. Note that $\mathbf{H}_{t,0} = \mathbf{X}_t = (X_{t,1}, \dots, X_{t,N})$ and $\mathbf{H}_{t,I+1} = \Delta_t = (\Delta_t^{\min}, \Delta_t^{\max})$. The model assumes $I = 2$ or $I = 3$ hidden layers and outputs our peak load prediction targets: Δ_t^{\min} and Δ_t^{\max} . The model is regularized using input feature selection, a dropout layer, and L_1 regularization of the hidden layers and their weights. These methods are subject to tuning. We tune them along with other hyperparameters, such as the number of hidden layers, their activation functions, number of neurons, and the learning rate. We summarize all the hyperparameters to be tuned in the following list.

- Input feature selection as shown in Tab. 1 (21 hyperparameters).

³Absolute wind speed is defined as $\text{wind} = \sqrt{\text{windE}^2 + \text{windN}^2}$

⁴We are happy to provide them upon request.

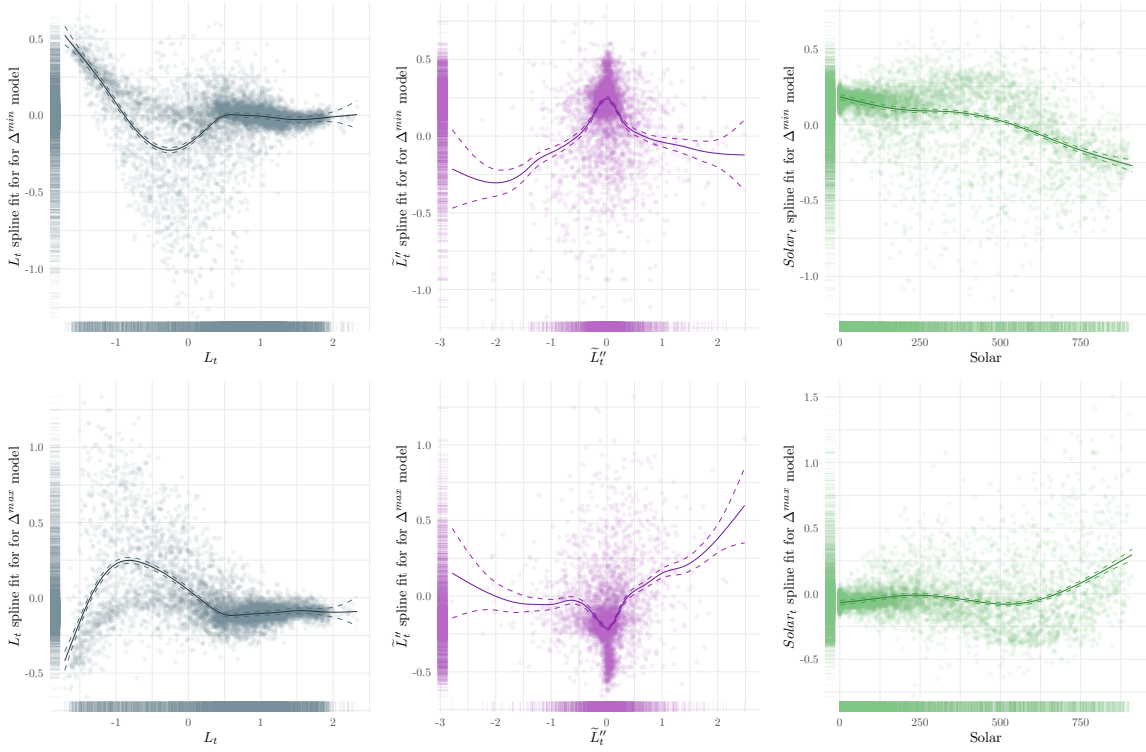


Figure 5: Fitted cubic B-splines of the simple GAM model (6) for Δ_t^{\min} (top) and Δ_t^{\max} (bottom) for L_t (left), \tilde{L}_t'' (center) and Solar_t (right).

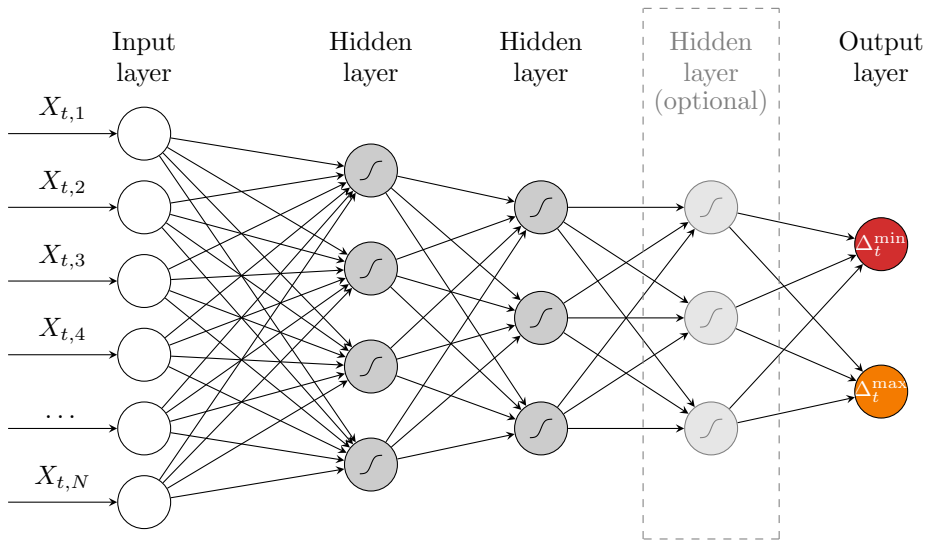


Figure 6: Exemplary network structure of the MLP.

- Number of hidden layers – either 2 or 3 (1 hyperparameter).
- Dropout layer – whether to use it after the input layer and if yes, at what rate.

The rate is drawn uniformly from $(0, 1)$ interval (up to 2 hyperparameters).

- Activation functions in the hidden layers. The possible functions are: elu, relu, sigmoid, softmax, softplus, and tanh (1 hyperparameter per layer).
- Number of neurons in the hidden layer drawn on an exp-scale from $[4, 128]$ interval (1 hyperparameter per layer).
- L_1 regularization – whether to use it on the hidden layers and their weights and if yes, at what rate. The rate is drawn on an exp-scale from $(10^{-5}, 10)$ interval (up to 4 hyperparameters per layer).
- Learning rate for the Adam optimization algorithm drawn on an exp-scale from $(10^{-5}, 10^{-1})$ interval (1 hyperparameter).

This results in up to 43 hyperparameters that are subject to tuning. However, the number of possible combinations is far too high to check every single value for each parameter. Thus, we use the Optuna [42] tool for the tuning exercise. It utilizes a Bayesian optimization algorithm to find the optimal parameters. The number of tuning iterations is set to 1000. Each iteration consists of a small, 3-steps expanding window study. In the first step, we consider in-sample data excluding the last three months, and we fit the model to that. Then, using the model, we predict the values for the following month. In the second step, we roll our window by one month, this time including the one that we predicted in the previous step, and repeat the fitting and predicting exercise. The third step is analogous to the second one. This way, we obtain the predictions of the recent three months of in-sample data with the given set of hyperparameters. To mimic the prediction study, we could tune the hyperparameters only using the most recent month. However, we use three of them for the sake of robustness, i.e., we want to avoid an overfitted deep neural network. After the whole iteration, the MSE of the predictions is calculated, and the Optuna sampler seeks the hyperparameter set that minimizes this value. The tuning procedure is repeated every month, i.e., before each modeling for the following month, resulting in 12 hyperparameter tunings.

The model is constructed and estimated with the Tensorflow [43] and Keras [44] framework. In addition to the tuned parameters, we arbitrarily set the validation set size to 25% of the input data, the maximum number of epochs to 1500, and the batch size to $7 \cdot 48 = 336$. Moreover, we use the Adam optimizing algorithm, MSE as the loss function, and the early stopping callback with a patience of 50 epochs. Naturally, the input data is standardized prior to the modeling.

Due to the stochastic nature of the DNNs, we may face instability between multiple estimations of a single DNN. Therefore, the predictions are obtained each time using an ensemble of predictions provided by ten runs of each of the five best hyperparameter sets. Ensembling is sometimes also called forecast averaging and has been applied to electricity price [45] and load forecasting [46] before. Thus, a single prediction represents an ensemble (here the mean) of 50 independent ones.

4. Empirical study and results

4.1. GAM parameter significance

Tab. 2 shows parameter significance estimates of the reduced GAM model **GAM.red** (5). We only report single terms and interactions with cumulative effective degrees of freedom (EDF) larger than 3 for the single terms and larger than 6 for the interactions to keep the table concise. The table also reports the F-statistic for an F-test that evaluates the joint significance with respect to no effect of the model term. We do not report the p-value here since all variables included in Tab. 2 are very close to 0. Large EDF values and F-statistics indicate the high importance of the corresponding model term.

We observe that L_t is by far the most important input as a single term, but also in the interactions. This holds for both minimum and maximum models. Besides, we also see that various non-linear effects, represented by the tensor interactions, receive high EDF values. Overall, minimum and maximum models differ in various respects. However, the (lagged and modified) second derivatives of the load \tilde{L}_{t+k} receive high EDF values in both models. A similar conclusion can be made for the weather variables and interactions with the weather. Solar is clearly the most important among the weather variables, but temperature, wind, and humidity also contribute. Those weather effects are known to have some relevance in load forecasting literature as well [12, 10, 15].

4.2. DNN Hyperparameter tuning results

We conduct the DNN hyperparameter tuning 12 times and each time we choose 5 best sets what results in 60 sets in total. Fig. 7 presents the choice frequency of input features in the obtained sets.

The most important inputs are L_t , \tilde{L}_{t+1}'' and Solar, which is similar to the parameter importance in the **GAM.red** model, see Tab. 2. The least important variables are \tilde{L}_{t-4}'' and WindN. The DNN uses three hidden layers in 60% of cases and two in 40% of cases. On average, the first hidden layer consists of 66 neurons, the second and the third (if present) of 38. Fig. 9 presents the dependency between the numbers on different layers. Interestingly, the 2-layer networks tend to be smaller in the number of neurons than the 3-layer ones.

Fig 8 presents how often particular activation functions were chosen in each of the layers. We see that the elu function was chosen in half of the first layers, but in none of the remaining layers. The relu function is equally distributed across the first two layers and dominates the third layer. The most often chosen activation function in layer 2 is the softmax. The regularization frequency through dropout and L_1 regularization is reported in Fig. 10. We observe that, in most cases, the most optimal networks neglected these ways of regularization. Only the L_1 regularization of layer two was used in more than half of the tuned networks.

4.3. Study design

We evaluate the proposed models in an empirical evaluation study. The competitive models under consideration are the full GAM model **GAM.full** (4), the reduced GAM

Minimum			Maximum		
Single Terms	EDF	F	Single Terms	EDF	F
L_t	9.5	8.9	L_t	10.8	17.6
\tilde{L}_{t-1}''	8.8	4.4	\tilde{L}_{t-2}''	6.7	4.9
\tilde{L}_{t+1}''	8.4	4.8	L_{t-1}	6.3	6.9
\tilde{L}_t''	8.2	4.6	L_{t+1}	5.4	5.0
Humid	6.1	3.7	D_t	4.8	3.1
WindE	5.1	8.9	Temp	4.1	11.5
A_t	4.7	4.9	Solar	4.0	5.5
WindN	4.2	8.5	WindE	3.8	5.8
Temp	3.5	3.6	\tilde{L}_{t+4}''	3.2	2.1
L_{t-1}	3.3	1.3	\tilde{L}_{t+1}''	3.1	2.2
Interactions	EDF	F	Interactions	EDF	F
L_t, A_t	26.7	7.8	L_t, A_t	37.8	28.1
L_t, Solar	20.7	11.2	L_t, D_t	25.1	20.6
L_t, D_t	18.3	8.2	Solar, A_t	15.4	6.4
L_t, L_{t+1}	17.1	4.0	$\tilde{L}_t'', \tilde{L}_{t-1}''$	14.9	6.5
$\tilde{L}_t'', \tilde{L}_{t-1}''$	13.5	2.5	Solar, D_t	11.0	8.5
L_t, Temp	13.3	3.1	$\tilde{L}_t'', \tilde{L}_{t+1}''$	11.0	2.4
L_t, L_{t-1}	13.0	4.9	$\tilde{L}_t'', \tilde{L}_{t+2}''$	10.7	2.8
$\tilde{L}_t'', \tilde{L}_{t+1}''$	12.1	2.3	L_t, Solar	10.0	2.9
L_t, W_t	11.7	3.0	$\tilde{L}_t'', \text{Temp}$	9.5	3.4
$\tilde{L}_t'', \tilde{L}_{t+2}''$	11.4	2.9	L_t, WindE	9.3	2.5
L_t, Humid	10.1	2.6	L_t, \tilde{L}_{t-4}''	9.1	2.1
$\tilde{L}_t'', \tilde{L}_{t-3}''$	9.9	3.1	$\tilde{L}_t'', \tilde{L}_{t-3}''$	9.0	2.2
L_t, WindN	9.9	4.4	$\text{Solar}, \text{WindE}$	9.0	2.5
$\tilde{L}_t'', \text{Humid}$	9.8	1.8	L_t, W_t	8.9	1.9
$\tilde{L}_t'', \tilde{L}_{t-2}''$	9.3	2.1	L_t, \tilde{L}_{t-3}''	8.7	1.5
L_{t+1}, Solar	8.3	1.3	L_t, L_{t+1}	8.4	1.3
Solar, D_t	8.2	2.0	L_t, \tilde{L}_{t+3}''	7.4	1.3
L_t, WindE	7.6	2.5	L_t, \tilde{L}_{t+1}''	6.8	1.5
$\text{Solar}, \text{WindE}$	6.9	1.6	L_t, \tilde{L}_{t-1}''	6.5	1.4
$\tilde{L}_t'', \text{WindE}$	6.9	1.5	L_t, \tilde{L}_{t+4}''	6.1	1.0
L_t, \tilde{L}_{t+1}''	6.2	4.2			

Table 2: Effective degree of freedom and F-statistic of selected model terms of model **GAM.red**.

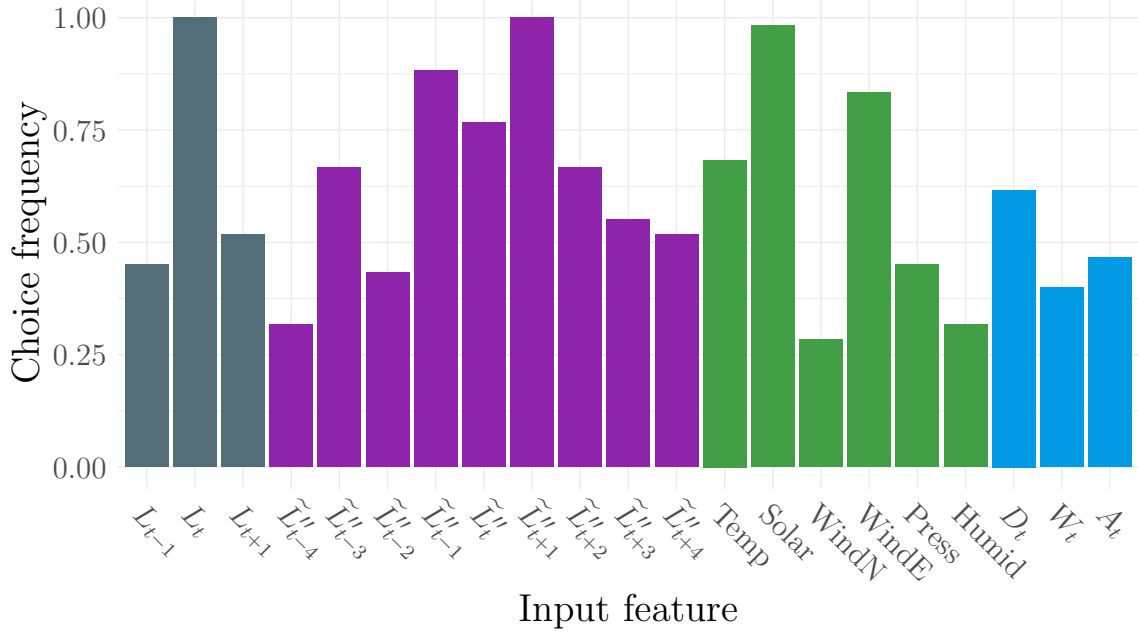


Figure 7: Input choice frequency in the best 60 DNN hyperparameter sets.

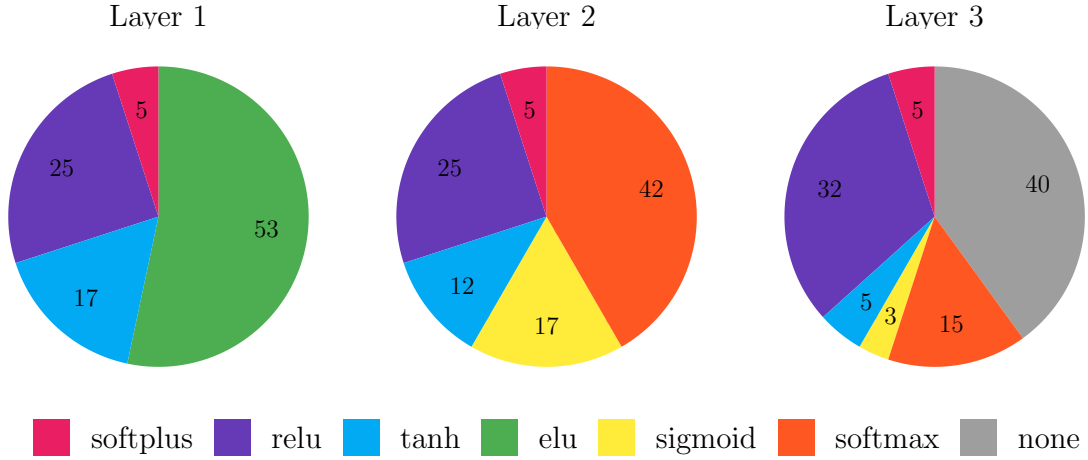


Figure 8: Share of chosen activation functions in the best 60 DNN hyperparameter sets in %.

model **GAM.red** (5), and the deep neural network **DNN** (7). Combining sophisticated models often improves predictive accuracy, thus we also consider the naive combination of **GAM.full**, **GAM.red** and **DNN**. The naive combination uses uniform weights for the three models.

Additionally, we consider the simple GAM model **GAM.simple** (6), the full GAM model (4) without weather inputs **GAM.noWeather**, and the naive benchmark **Naive** defined by $\tilde{L}_t^{\max} = L_t$ and $\tilde{L}_t^{\min} = L_t$ for comparison purposes.

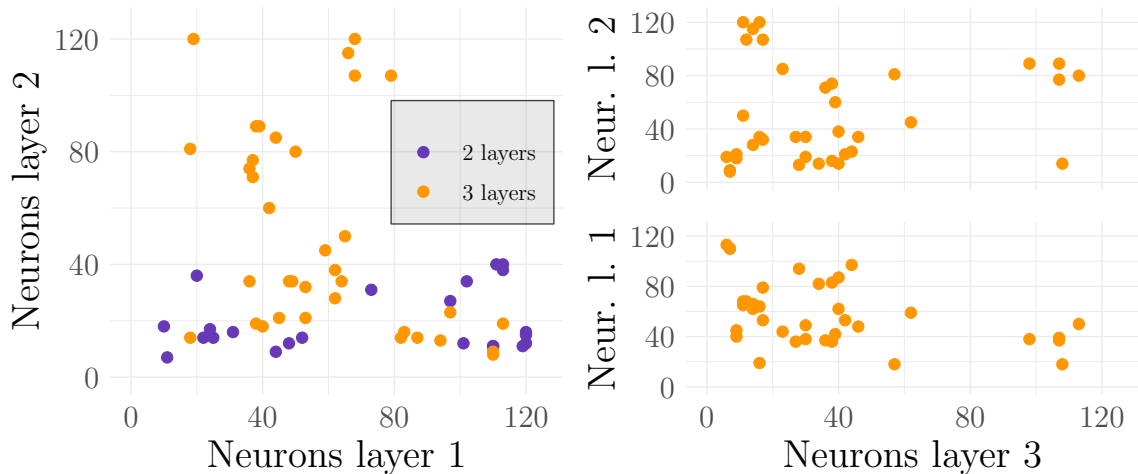


Figure 9: Neurons per layer in the best 60 DNN hyperparameter sets.

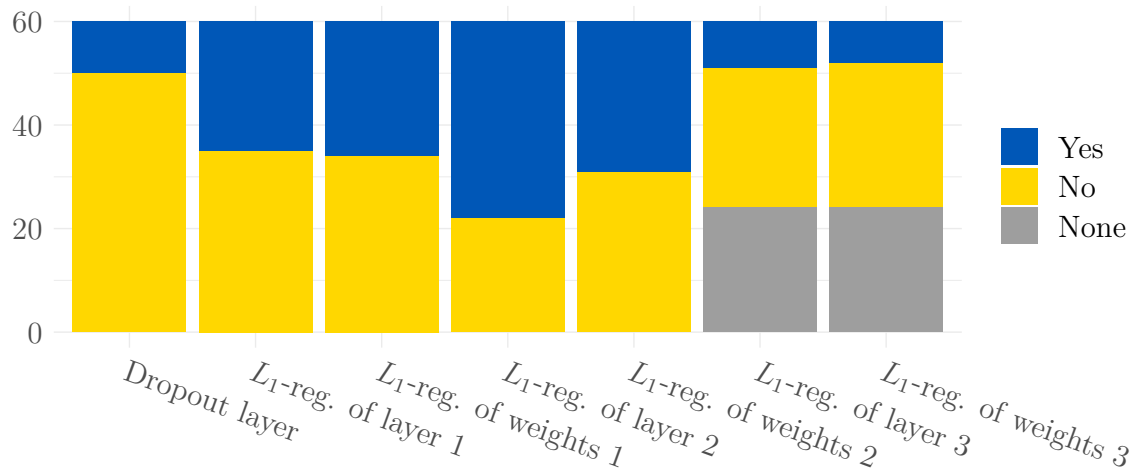


Figure 10: Regularization frequency in the best 60 DNN hyperparameter sets.

As mentioned, we evaluate the predictive accuracy of the models in a rolling window study, measuring the performance in the 12 months from 10/2020 to 09/2021. We evaluate the predictions by calculating the root mean squared error (RMSE) of the predictions. Here, we distinguish a joint RMSE and an RMSE for the minimum and maximum:

$$\text{RMSE} = \sqrt{\sum_{t \in \mathbb{T}} (\tilde{L}_t^{\min} - L_t^{\min})^2 + (\tilde{L}_t^{\max} - L_t^{\max})^2} \quad (8)$$

$$\text{RMSE}_m = \sqrt{\sum_{t \in \mathbb{T}} (\tilde{L}_t^m - L_t^m)^2} \quad (9)$$

where $m \in \{\min, \max\}$ and \mathbb{T} represents the index set of time points of the considered

Overall	20/10	20/11	20/12	21/1	21/2	21/3	21/4	21/5	21/6	21/7	21/8	21/9	Avg
GAM.full	.1239 (56.3)	.0703 (58.5)	.0497 (56.6)	.0532 (57.6)	.0988 (55.4)	.1202 (57.8)	.1447 (57.2)	.1746 (56.7)	.1368 (56.3)	.1537 (53.9)	.1383 (60.2)	.1163 (56.9)	.1150 (56.9)
GAM.red	.1241 (56.2)	.0700 (58.7)	.0496 (56.6)	.0536 (57.3)	.0994 (55.2)	.1201 (57.8)	.1467 (56.6)	.1750 (56.6)	.1385 (55.8)	.1554 (53.4)	.1374 (60.5)	.1162 (56.9)	.1155 (56.7)
DNN	.1230 (56.6)	.0704 (58.4)	.0507 (55.7)	.0545 (56.6)	.1027 (53.7)	.1251 (56.1)	.1514 (55.2)	.1653 (59.0)	.1474 (52.9)	.1538 (53.9)	.1422 (59.1)	.1225 (54.6)	.1174 (56.0)
Combination	.1221 (56.9)	.0689 (59.3)	.0491 (57.1)	.0527 (58.0)	.0979 (55.8)	.1193 (58.1)	.1443 (57.3)	.1684 (58.2)	.1365 (56.4)	.1512 (54.6)	.1371 (60.6)	.1164 (56.9)	.1137 (57.4)
GAM.noWeather	.1301 (54.1)	.0707 (58.2)	.0508 (55.6)	.0533 (57.5)	.1058 (52.3)	.1253 (56.0)	.1471 (56.5)	.1822 (54.8)	.1401 (55.3)	.1584 (52.5)	.1424 (59.1)	.1249 (53.7)	.1193 (55.3)
GAM.simple	.1531 (46.0)	.0940 (44.5)	.0584 (49.0)	.0672 (46.5)	.1267 (42.9)	.1500 (47.3)	.1797 (46.8)	.2093 (48.1)	.1733 (44.7)	.1873 (43.8)	.1671 (52.0)	.1413 (47.6)	.1423 (46.7)
Naive	.2833	.1693	.1144	.1255	.2217	.2847	.3380	.4029	.3131	.3334	.3478	.2699	.2670

Table 3: RMSE values for peak load prediction in MW in the evaluation study with corresponding averages (last column). Relative improvements over the **Naive** model in % are in brackets below.

month. The naive benchmark model was also used in the competition skill score which corresponds to the relative improvement in the RMSE:

$$\text{Score} = \text{RMSE}(\text{Model})/\text{RMSE}(\text{naive}). \quad (10)$$

4.4. Evaluation results

Tab. 3 shows the RMSE and corresponding score results of the considered models. Overall, we see that all sophisticated models show high predictive accuracy. The **GAM.full** and **GAM.red** have almost the same predictive accuracy and improve the RMSE of **naive** by about 57%. The **DNN** model performs only slightly worse with an accuracy improvement of 56%. Still, we see a few months where **DNN** outperforms the GAM models, namely October 2020 and May 2021. Hence, the **Combination** has a robust predictive accuracy and exhibits another small improvement over the individual models. This improvement is about 57.5% compared to **naive**. We want to mention that in the WPD challenge, the test month was September 2021. Here, the GAM models performed particularly well with a skill score of 43.1% (56.9% Improvement compared to **naive**) - the same score as the more robust **Combination** model. In the competition, we used a slightly modified combination model (e.g., the GAM also included manually selected 3-way interactions) with a final skill score of 42.6% (57.4% Improvement compared to **naive**). The second and third-placed teams (*WOJJ* and *code.green*) received a score of 43.6% and 43.7%. Thus, the proposed **Combination** model has an improvement of more than 1 percentage point in terms of RMSE compared to the other teams.

From the **GAM.noWeather** model in Tab. 3 we can deduce that the weather variables improve the RMSE skill score by 1.6 percentage points on average. This sounds minor, but it is substantial, considering that the difference in the skill score between **GAM.simple** and **GAM.full** is only about 10 percentage points.

	20/10	20/11	20/12	21/1	21/2	21/3	21/4	21/5	21/6	21/7	21/8	21/9	Avg
Min													
GAM.full	.1551	.0831	.0544	.0593	.1136	.1281	.1429	.1824	.1389	.1658	.1528	.1169	.1244
GAM.red	.1529	.0826	.0543	.0598	.1151	.1278	.1452	.1801	.1416	.1673	.1513	.1188	.1247
DNN	.1513	.0838	.0565	.0630	.1176	.1373	.1518	.1746	.1527	.1684	.1579	.1297	.1287
Combination	.1517	.0818	.0541	.0596	.1132	.1285	.1433	.1761	.1404	.1644	.1520	.1197	.1237
GAM.noWeather	.1635	.0827	.0545	.0592	.1181	.1306	.1463	.1869	.1434	.1694	.1571	.1243	.1280
GAM.simple	.1889	.1105	.0623	.0758	.1413	.1624	.1768	.2122	.1817	.1963	.1842	.1443	.1531
Naive	.3256	.1890	.1196	.1305	.2375	.3010	.3330	.4131	.3269	.3468	.3691	.2723	.2804
Max													
GAM.full	.0816	.0545	.0444	.0462	.0813	.1116	.1464	.1663	.1346	.1406	.1220	.1156	.1038
GAM.red	.0860	.0544	.0444	.0466	.0805	.1120	.1481	.1698	.1353	.1425	.1220	.1135	.1046
DNN	.0859	.0538	.0440	.0445	.0853	.1115	.1511	.1555	.1418	.1377	.1247	.1149	.1042
Combination	.0824	.0529	.0434	.0446	.0797	.1094	.1453	.1603	.1324	.1366	.1203	.1129	.1017
GAM.noWeather	.0842	.0561	.0469	.0466	.0918	.1197	.1478	.1774	.1367	.1466	.1259	.1255	.1088
GAM.simple	.1057	.0740	.0541	.0574	.1101	.1365	.1825	.2065	.1645	.1780	.1481	.1381	.1296
Naive	.2335	.1469	.1090	.1203	.2047	.2674	.3429	.3925	.2986	.3193	.3252	.2675	.2523

Table 4: $RMSE_{\min}$ and $RMSE_{\max}$ values for the minimum and maximum peak load in MW for considered prediction models in the evaluation study with corresponding average (last column).

Tab. 4 presents the $RMSE_{\min}$ and $RMSE_{\max}$ results. We observe that the performance between the GAM models and the DNN varies with the prediction target. For the minimum peak load models, the DNN performs clearly worse than the GAM models, even worse than the **GAM.noWeather** model. Thus, the predictive accuracy of the **Combination** model improves only marginally compared to the well-performing GAM models **GAM.full** and **GAM.red**. In contrast, the neural network model performs similarly to the two GAM models for the maximum peak load. Thus, we see a substantial increase in predictive accuracy due to aggregation in the **Combination** model.

5. Conclusion

This paper covers estimating high-resolution electricity peak demand given lower resolution data. For this purpose, we developed models using two distinct model classes, namely **GAM** and **DNN**. Combining these models received the best score in the WPD data competition. The month to predict in the competition was September 2021. However, to evaluate the robustness of our proposed methodology, we report model performance for eleven additional months. The model components and their importance were discussed in detail. Given the results, we conclude that the most important ones are the load L_t , its modified second derivative \tilde{L}_t'' , and Solar. This applies to both **GAM** and **DNN** models. The proposed combination of both model classes improves performance and delivers more robust predictions. The method was proven in a robust 12-months evaluation study. Overall, this combination yields an RMSE

that is 1.2% lower compared to the best performing individual model **GAM.full** and 57.4% lower compared to the **Naive** benchmark. Including weather information was clearly beneficial. Comparing **GAM.full** to **GAM.noWeather** shows that considering weather variables improves the RMSE by 1.6 percentage points on average. The proposed methodology can easily be applied to different substations. An interesting question is how the model performance changes when the data is from a different region. If the results generalize well, network operators would not need to pay for collecting high-resolution data in the first place. The high-resolution features of interest could be extracted from low-resolution data using the proposed methods. This is an interesting topic for future work.

References

- [1] J. Zheng, D. W. Gao, L. Lin, Smart meters in smart grid: An overview, in: 2013 IEEE Green Technologies Conference (GreenTech), IEEE, 2013, pp. 57–64.
- [2] M. Sănduleac, I. Ciornei, L. Toma, R. Plămnescu, A.-M. Dumitrescu, M. M. Albu, High reporting rate smart metering data for enhanced grid monitoring and services for energy communities, *IEEE Transactions on Industrial Informatics* 18 (6) (2021) 4039–4048.
- [3] N. Mughees, S. A. Mohsin, A. Mughees, A. Mughees, Deep sequence to sequence bi-lstm neural networks for day-ahead peak load forecasting, *Expert Systems with Applications* 175 (2021) 114844.
- [4] J. Lee, Y. Cho, National-scale electricity peak load forecasting: Traditional, machine learning, or hybrid model?, *Energy* 239 (2022) 122366.
- [5] M. Uddin, M. F. Romlie, M. F. Abdullah, S. Abd Halim, T. C. Kwang, et al., A review on peak load shaving strategies, *Renewable and Sustainable Energy Reviews* 82 (2018) 3323–3332.
- [6] P. Lissa, C. Deane, M. Schukat, F. Seri, M. Keane, E. Barrett, Deep reinforcement learning for home energy management system control, *Energy and AI* 3 (2021) 100043.
- [7] M. Sun, Y. Wang, G. Strbac, C. Kang, Probabilistic peak load estimation in smart cities using smart meter data, *IEEE Transactions on Industrial Electronics* 66 (2) (2018) 1608–1618.
- [8] J.-S. Chou, D.-S. Tran, Forecasting energy consumption time series using machine learning techniques based on usage patterns of residential householders, *Energy* 165 (2018) 709–726.

- [9] Y. Chen, P. Xu, Y. Chu, W. Li, Y. Wu, L. Ni, Y. Bao, K. Wang, Short-term electrical load forecasting using the Support Vector Regression (SVR) model to calculate the demand response baseline for office buildings, *Applied Energy* 195 (2017) 659–670.
- [10] S. Haben, G. Giasemidis, F. Ziel, S. Arora, Short term load forecasting and the effect of temperature at the low voltage level, *International Journal of Forecasting* 35 (4) (2019) 1469–1484.
- [11] Z. Guo, K. Zhou, X. Zhang, S. Yang, A deep learning model for short-term power load and probability density forecasting, *Energy* 160 (2018) 1186–1200.
- [12] J. Xie, Y. Chen, T. Hong, T. D. Laing, Relative humidity for load forecasting models, *IEEE Transactions on Smart Grid* 9 (1) (2016) 191–198.
- [13] V. Dehalwar, A. Kalam, M. L. Kolhe, A. Zayegh, Electricity load forecasting for urban area using weather forecast information, in: *2016 IEEE International Conference on Power and Renewable Energy (ICPRE)*, IEEE, 2016, pp. 355–359.
- [14] M. Cai, M. Pipattanasomporn, S. Rahman, Day-ahead building-level load forecasts using deep learning vs. traditional time-series techniques, *Applied energy* 236 (2019) 1078–1088.
- [15] S. Muzaffar, A. Afshari, Short-term load forecasts using LSTM networks, *Energy Procedia* 158 (2019) 2922–2927.
- [16] H. Acaroğlu, F. P. García Márquez, Comprehensive review on electricity market price and load forecasting based on wind energy, *Energies* 14 (22) (2021) 7473.
- [17] T. Hong, P. Wang, L. White, Weather station selection for electric load forecasting, *International Journal of Forecasting* 31 (2) (2015) 286–295.
- [18] D. H. Vu, K. M. Muttaqi, A. P. Agalgaonkar, A. Bouzerdoum, Short-term electricity demand forecasting using autoregressive based time varying model incorporating representative data adjustment, *Applied Energy* 205 (2017) 790–801.
- [19] E. Aguilar Madrid, N. Antonio, Short-term electricity load forecasting with machine learning, *Information* 12 (2) (2021) 50.
- [20] X. Zhang, J. Wang, K. Zhang, Short-term electric load forecasting based on singular spectrum analysis and support vector machine optimized by Cuckoo search algorithm, *Electric Power Systems Research* 146 (2017) 270–285.
- [21] F. Sheng, L. Jia, Short-term load forecasting based on SARIMAX-LSTM, in: *2020 5th International Conference on Power and Renewable Energy (ICPRE)*, IEEE, 2020, pp. 90–94.

- [22] G.-F. Fan, M. Yu, S.-Q. Dong, Y.-H. Yeh, W.-C. Hong, Forecasting short-term electricity load using hybrid support vector regression with grey catastrophe and random forest modeling, *Utilities Policy* 73 (2021) 101294.
- [23] A. Pierrot, Y. Goude, Short-term electricity load forecasting with generalized additive models, *Proceedings of ISAP power* 2011.
- [24] Y. Goude, R. Nedellec, N. Kong, Local short and middle term electricity load forecasting with semi-parametric additive models, *IEEE transactions on smart grid* 5 (1) (2013) 440–446.
- [25] F. Ziel, Smoothed bernstein online aggregation for short-term load forecasting in iee dataport competition on day-ahead electricity demand forecasting: Post-covid paradigm, *IEEE Open Access Journal of Power and Energy*.
- [26] U. Amato, A. Antoniadis, I. De Feis, Y. Goude, A. Lagache, Forecasting high resolution electricity demand data with additive models including smooth and jagged components, *International Journal of Forecasting* 37 (1) (2021) 171–185.
- [27] M. B. Tasre, P. P. Bedekar, V. N. Ghate, Daily peak load forecasting using ANN, in: *2011 Nirma University International Conference on Engineering*, IEEE, 2011, pp. 1–6.
- [28] F. Pallonetto, C. Jin, E. Mangina, Forecast electricity demand in commercial building with machine learning models to enable demand response programs, *Energy and AI* 7 (2022) 100121.
- [29] S. Hosein, P. Hosein, Load forecasting using deep neural networks, in: *2017 IEEE Power & Energy Society Innovative Smart Grid Technologies Conference (ISGT)*, IEEE, 2017, pp. 1–5.
- [30] K. Amarasinghe, D. L. Marino, M. Manic, Deep neural networks for energy load forecasting, in: *2017 IEEE 26th International Symposium on Industrial Electronics (ISIE)*, IEEE, 2017, pp. 1483–1488.
- [31] A. S. Khwaja, A. Anpalagan, M. Naeem, B. Venkatesh, Joint bagged-boosted artificial neural networks: Using ensemble machine learning to improve short-term electricity load forecasting, *Electric Power Systems Research* 179 (2020) 106080.
- [32] T. Walser, A. Sauer, Typical load profile-supported convolutional neural network for short-term load forecasting in the industrial sector, *Energy and AI* 5 (2021) 100104.
- [33] G. Memarzadeh, F. Keynia, Short-term electricity load and price forecasting by a new optimal lstm-nn based prediction algorithm, *Electric Power Systems Research* 192 (2021) 106995.

- [34] A. Shaqour, T. Ono, A. Hagishima, H. Farzaneh, Electrical demand aggregation effects on the performance of deep learning-based short-term load forecasting of a residential building, *Energy and AI* 8 (2022) 100141.
- [35] T. Bashir, C. Haoyong, M. F. Tahir, Z. Liqiang, Short term electricity load forecasting using hybrid prophet-lstm model optimized by bpnn, *Energy Reports* 8 (2022) 1678–1686.
- [36] Z. A. Khan, A. Ullah, I. U. Haq, M. Hamdy, G. M. Maurod, K. Muhammad, M. Hijji, S. W. Baik, Efficient short-term electricity load forecasting for effective energy management, *Sustainable Energy Technologies and Assessments* 53 (2022) 102337.
- [37] T. Gneiting, Making and evaluating point forecasts, *Journal of the American Statistical Association* 106 (494) (2011) 746–762.
- [38] G. J. Székely, M. L. Rizzo, N. K. Bakirov, Measuring and testing dependence by correlation of distances, *The annals of statistics* 35 (6) (2007) 2769–2794.
- [39] F. Ziel, M5 competition uncertainty: Overdispersion, distributional forecasting, gamlss, and beyond, *International Journal of Forecasting*.
- [40] A. März, T. Kneib, Distributional gradient boosting machines, arXiv preprint arXiv:2204.00778.
- [41] S. Wood, *Generalized Additive Models: An Introduction with R*, 2nd Edition, Chapman and Hall/CRC, 2017.
- [42] T. Akiba, S. Sano, T. Yanase, T. Ohta, M. Koyama, Optuna: A next-generation hyperparameter optimization framework, in: *Proceedings of the 25th ACM SIGKDD international conference on knowledge discovery & data mining*, 2019, pp. 2623–2631.
- [43] M. Abadi, A. Agarwal, P. Barham, E. Brevdo, Z. Chen, C. Citro, G. S. Corrado, A. Davis, J. Dean, M. Devin, S. Ghemawat, I. Goodfellow, A. Harp, G. Irving, M. Isard, Y. Jia, R. Jozefowicz, L. Kaiser, M. Kudlur, J. Levenberg, D. Mané, R. Monga, S. Moore, D. Murray, C. Olah, M. Schuster, J. Shlens, B. Steiner, I. Sutskever, K. Talwar, P. Tucker, V. Vanhoucke, V. Vasudevan, F. Viégas, O. Vinyals, P. Warden, M. Wattenberg, M. Wicke, Y. Yu, X. Zheng, **TensorFlow: Large-Scale Machine Learning on Heterogeneous Systems**, software available from tensorflow.org (2015).
URL <https://www.tensorflow.org/>
- [44] F. Chollet, et al., Keras, <https://keras.io> (2015).

- [45] J. Lago, G. Marcjasz, B. De Schutter, R. Weron, Forecasting day-ahead electricity prices: A review of state-of-the-art algorithms, best practices and an open-access benchmark, *Applied Energy* 293 (2021) 116983.
- [46] H. Takeda, Y. Tamura, S. Sato, Using the ensemble kalman filter for electricity load forecasting and analysis, *Energy* 104 (2016) 184–198.